Conference Paper, Published Version

Sung-Uk, Choi; Wonjun, Yang

Numerical Simulations of 3-D Flows Around Bridge Piers

Numerical Simulations of 3-D Flows Around Bridge Piers

By

Choi, Sung-Uk[1] and Yang, Wonjun[2]

ABSTRACT

In the present paper, the numerical simulations of the 3D flows around the bridge pier are presented. The LES and the RNG k-ε model are used for the numerical analysis of Navier-Stokes equations. Flows without and with the scour hole are simulated and compared with measured data from the experiments by Melville and Raudkivi (1977). The computed flow patterns appear to agree well with the observed patterns. However, the LES is shown to reproduce the vortex at the upstream part of the pier much better than the RNG k-ε model. Using the computed results, the downflow occurring at the frontal part of the pier is also investigated. At the location far from the pier, the downflow computed by the LES seem to be similar to that by the RNG k-ε model. However, near the pier, the downflow by the LES is observed to be much stronger than that by the RNG k-ε model.

INTRODUCTION

The flow phenomenon related with the local scour around the bridge pier is extremely complicated, and it is characterized by highly 3D turbulent motions. The downflow, the horseshoe vortex, and the wake vortex are known to be responsible for the local scour. The complex nature of flow has prevented the hydraulic engineers from applying the hydrodynamic model to this problem.

[1] Associate Prof., Department of Civil Engineering, Yonsei University, Seoul, Korea, (schoi@yonsei.ac.kr)
[2] Graduate Student, Department of Civil Engineering, Yonsei University, Seoul, Korea

Therefore, previous methods to predict the scour depth are empirical relationships such as CSU and Laursen formulas.

Recent development in computational fluid dynamics enables the hydraulic engineers to study the local scour around the bridge pier based on hydrodynamics. Olsen and Melaaen (1993) solved the Reynolds equations with the *k*-ε model for turbulence closure. Considering both suspended load and bedload, they solved the bed sediment conservation equation by iterating the procedure until the scour hole at an equilibrium state is obtained. Richardson and Panchang (1998) simulated the flow structures around a bridge pier with and without the scour hole. They used FLOW3D with the RNG k-ε model. Comparing the simulated with the experimental results, they found that the 3D hydrodynamic model simulates well the complex flow patterns around the bridge pier. Wang and Jia (2000) simulated an evolution of the scour hole developing around the bridge pier by using CCHE3D. In the computations, they used empirical functions for sediment transport, which were calibrated by using the experimental data. Li and Lin (2000) performed the LES to study the flow structures around a rectangular pier. They carried out the spectral analysis of turbulent and coherent structures. Tseng et al. (2000) conducted the numerical simulation with the square and the circular piers by the LES. They found that the downflow is made at the front face of the pier and this affects the creation of the horseshoe vortex. They also compared turbulent structures, lift coefficient, and drag coefficient with the experimental results, and obtained good agreements.

This paper presents an application of the 3D hydrodynamic model to the flow around the bridge pier. Herein FLOW3D is used (Sicilian et al., 1987), which solves time-dependent 3D Navier-Stokes equations by the volume-of-fluid method (Hirt and Nichols, 1981). Many techniques of turbulence modeling are available in FLOW3D. We employed the LES (Large Eddy Simulation) technique to both cases without and with the scour hole. We also use the RNG (Renormalization Group) k-ε model to see the impact from the non-isotropic turbulence assumption. First, the flowfields are simulated and compared with the measured data. Then, the downflow characteristics are investigated.

LARGE EDDY SIMULATION

The spatially-filtered Navier-Stokes equations for fluid motion are given by

$$\frac{\partial \overline{u_i}}{\partial x_i} = 0$$

$$\frac{\partial \overline{u_i}}{\partial t} + \frac{\partial}{\partial x_j}\overline{U_i U_j} = -\frac{1}{\rho}\frac{\partial \overline{p}}{\partial x_i} + \nu \frac{\partial^2 \overline{u}_i}{\partial x_j \partial x_j}$$

where U_i is the *i*-component of instantaneous velocity, $\overline{u}_i$ and $\overline{p}$ are the spatially-filtered value of U_i and pressure, respectively, ρ is the density of water, and ν is the kinematic viscosity. In the above equations, the overbar denotes the spatially-filtered value. Expanding the non-linear advective term in the momentum equation leads to

$$\overline{U_i U_j} = \overline{\overline{u}_i \overline{u}_j} + \overline{u_i' \overline{u}_j} + \overline{\overline{u}_i u_j'} + \overline{u_i' u_j'}$$

If we define the residual stress term by $\tau_{ij}^R = u_i' \overline{u}_j + \overline{u}_i u_j' + u_i' u_j'$, then we have the non-linear advective term such as

$$\frac{\partial}{\partial x_j}(\overline{U_i U_j}) = \frac{\partial}{\partial x_j}(\overline{u}_i \overline{u}_j) + \frac{\partial}{\partial x_j}(\overline{\tau}_{ij}^R)$$

Substituting the advection term into the momentum equation, we have the following form of the momentum equation:

$$\frac{\partial \overline{u}_i}{\partial t} + \frac{\partial}{\partial x_j}\left(\overline{u}_i \overline{u}_j\right) = -\frac{1}{\rho}\frac{\partial \overline{p}}{\partial x_i} + \nu \frac{\partial^2 \overline{u}_i}{\partial x_j \partial x_j} - \frac{\partial}{\partial x_j}\overline{\tau}_{ij}^r$$

where τ_{ij}^r is the deviatoric residual stress tensor defined by

$$\tau_{ij}^r = \tau_{ij}^R - \frac{2}{3} k_r \delta_{ij}$$

where k_r is the residual kinetic energy (= $1/2\tau_{ii}^R$) and δ_{ij} is the Kronecker delta. The Smagorinsky's (1963) model expresses the deviatoric residual stress tensor such as

$$\tau_{ij}^r = -2\nu_r \overline{S}_{ij}$$

where $\overline{S}_{ij}$ and ν_r are the strain rate and the turbulent viscosity of the filtered velocity. The mixing length model can be used to obtain the turbulent viscosity

of the filtered velocity, i.e.,

$$\nu_r = l_S^2 \bar{S}$$

where l_S is the characteristic length and $\bar{S}$ is the filtered characteristic strain rate ($=\left(2\bar{S}_{ij}\bar{S}_{ij}\right)^{1/2}$). In the above equation, the characteristic length is given by

$$l_S = C_S \Delta$$

where Δ is the filter size and C_S is the Smagorinsky coefficient (= 0.1).

RNG k-ε MODEL

The RNG *k*-*ε* model is known to require less reliance on empirical coefficients and provide a better solution in areas affected by high shear (Versteeg and Malalasekera, 1995). The RNG *k*-*ε* model developed by Yakhot et al. (1992) represents the effects of the small-scale turbulence by means of a random forcing function in the Reynolds equations. The RNG procedure systematically removes the small-scale motion from the governing equations by expressing their effects in terms of larger-scale motions and a modified viscosity. The equations of the time-averaged turbulent kinetic energy (*k*) and the dissipation rate (ε) of *k* are respectively given by (the tilde denotes the time-averaged value)

$$\frac{\partial k}{\partial t} + \frac{\partial}{\partial x_j}(k\tilde{u}_i) = \alpha_k \nu_{eff} \frac{\partial^2 k}{\partial x_j \partial x_j} + 2\nu_t E_{ij} \cdot E_{ij} - \varepsilon$$

$$\frac{\partial \varepsilon}{\partial t} + \frac{\partial}{\partial x_j}(\varepsilon\tilde{u}_i) = \alpha_k \nu_{eff} \frac{\partial^2 \varepsilon}{\partial x_j \partial x_j} + C_{1\varepsilon}^* \frac{\varepsilon}{k} 2\nu_t E_{ij} \cdot E_{ij} - C_{2\varepsilon} \frac{\varepsilon^2}{k}$$

where $\nu_{eff} = \nu + \nu_t$, $\nu_t = C_\mu k^2/\varepsilon$, $C_\mu =$ 0.0845, $\alpha_k = \alpha_\varepsilon =$ 1.39, $C_{1\varepsilon} =$ 1.42, $C_{2\varepsilon} =$ 1.68, $C_{1\varepsilon}^* = C_{1\varepsilon} - \eta(1-\eta/\eta_0)/1+\beta\eta^3$, $\eta = \left(2E_{ij} \cdot E_{ij}\right)^{1/2} k/\varepsilon$, $\eta_0 = 4.377$, and $\beta = 0.012$.

APPLICATIONS

Among the literatures published, Melville and Raudkivi (1977) provided perhaps the most detailed quantitative descriptions of the flow structures of the local scour. So, in this study, we perform the numerical simulations using the

experimental conditions in Melville and Raudkivi (1977). Fig. 1 shows the schematic figure of the flow condition used in the computation. Two cases are simulated separately, i.e., without and with the scour hole. Figs. 2(a) and (b) show the constructed grids for the cases without and with the scour hole, respectively. The number and size of the grids for each case are given in Table 1. Unfortunately, a detailed geometric description of the scour hole at the equilibrium state is not given in Melville and Raudkivi (1977). Thus, herein, the shape of the scour hole is approximated by a frustum of a cone, which is thought to be a good assumption at the upstream side of the pier (Richardson and Panchang, 1998).

Figs. 3(a)-(c) show the velocity vector fields at the vertical symmetry plane upstream of the pier. The computed results in Figs. 3(a) and (b) are from the LES and the RNG k-ε model, respectively, and Fig. 3(c) is the experimental data measured by Melville and Raudkivi (1977). In the figures, the velocity is made dimensionless by the mean approach velocity (u_o) of 0.25 m/s. It is seen that the computed and measured velocity fields show a similar flow pattern, i.e., the downflow is made along the upstream face of the pier. Compared with the measured profile, the magnitude of the downflow velocity from the numerical simulation is slightly small. Notice in Fig 3(a) that a return flow is observed nearly at the bottom. This cannot be decided to be realistic or not because the measurement is made on a too coarse grid.

The numerical simulations same as the previous ones are performed but the scour hole at the equilibrium state is included. The velocity vector fields made within the scour hole are presented in Figs. 4(a)-(c), where the first two figures are computed results by the LES and the RNG k-ε model, respectively, and the last is the measured data by Melville and Raudkivi (1977). Fig. 4(c) shows the flow descending into the scour hole along the vertical plane of symmetry and the formation of an eddy that constitutes the horseshow vortex. Among the two computed results, the LES is seen to simulate the formation of the eddy much better than the RNG k-ε model although the center of the vortex is located slightly downstream compared with Fig. 4(c).

Figs. 5(a)-(c) depict the distributions of the downflow velocity at the x-z plane parallel to the main flow direction. The distributions are given at three locations, i.e., x = 0.5D, 1D, and 2D. In the figures, both simulations without

and with the scour hole are presented, and the magnitude of the downflow velocity is made dimensionless by the mean approach velocity (u_o), and the distance from the bed by the uniform flow depth (h). In the figures, the minus downflow denotes vertically upward direction.

In the case without the scour hole, it is seen that the downflows by the LES and the RNG k-ε model are similar and negligible at $x = 2D$. However, as it is close to the pier, the profiles look differently and the maximum value of the downflow by the LES is seen to be larger than that by the RNG k-ε model. That is, as it gets close to the pier (at $x = 0.5D$), the downflow grows considerably and reaches a magnitude of $0.5u_o$ and $0.4u_o$ by the LES and by the RNG k-ε model, respectively.

In the case with the scour hole, the downflow profiles computed by the LES and the RNG k-ε model look very similar at $x = 1D$ and $2D$. However, at $x = 0.5D$, the downflow by the LES is seen to be much stronger than that by the RNG k-ε model. That is, the maximum values of w/u_o appear to be 0.6 and 0.2 by the LES and by the RNG k-ε model, respectively. This may indicate that the anisotropy of turbulence increases the strength of the downflow. Very recently, Graf and Istriarto (2001) performed laboratory experiments and showed that the maximum downflow reaches $0.6u_o$ at $x = 0.67D$, which coincides well with the results presented herein.

Fig. 6 shows the distribution of the downflow velocity at the y-z plane normal to the main flow direction. The profiles are provided at $0.5D$, $1D$, and $2D$. Like the previous cases, it is seen that the two simulated results look similar at $y = 2D$ but they look differently in the region close to the pier. In both cases (without and with the scour hole), the downflow velocity computed by the LES is larger than that by the RNG k-ε model.

CONCLUSIONS

This paper presented a 3D numerical simulation of the flow around the bridge pier. The Navier-Stokes equations were solved by using the LES and the RNG k-ε model. Flow patterns without and with the scour hole were simulated. We applied the numerical model to the experimental condition in Melville and Raudkivi (1977), and compared the computed results with their measured data.

Comparisons with the measured velocity fields revealed that the LES and the

RNG k-ε model are capable of computing the flow around the pier nicely. Specifically, the LES performed better than the RNG k-ε model in that it reproduces the vortex flow quite similarly with the observed data.

The downflow characteristics were also studied by using the simulated results. The computed downflows look similar at a distance far from the pier but, as it gets close to the pier, the maximum downflow by the LES appears larger than that by the RNG k-ε model. This may indicate that the non-isotropic nature of turbulence will increase the strength of the downflow.

ACKNOWLDEGMENT

This work was supported by grant No. 1991-1-311-002-3 from the Basic Research Program of the Korea Science & Engineering Foundation. Thanks are also due to Mr. Kiwon Hong in Soft-Tech International, Inc. in Korea for his technical support.

REFERENCES

1. Graf, W.H. and Istiarto, I. (2002). "Flow pattern in the scour hole around a cylinder." *Journal of Hydraulic Research*, IAHR, Vol. 40, No. 1, 13-20.
2. Hirt, C.W. and Nichols, B.D. (1981). "Volume of fluid (VOF) method for the dynamics of free boundaries." *Journal of Computational Physics*, Vol. 39, 201-225.
3. Li, C.W. and Lin, P. (2000). "Simulation of three-dimensional coherent and turbulent motions around a rectangular pile in an open channel flow." *Stochastic Hydraulics 2000*, Wang and Hu (eds), Beijing, China.
4. Melville, B.W. and Raudkivi, A.J. (1977). "Flow characteristics in local scour at bridge piers." *Journal of Hydraulic Research*, IAHR, Vol. 15, No. 4, 373-380.
5. Olsen, N.R.B. and Melaaen, M.C. (1993). "Three-dimensional calculation of scour around cylinders." *Journal of Hydraulic Engineering*, ASCE, Vol. 119, No. 9, 1048-1054.
6. Richardson, J.E. and Panchang, V.G. (1998). "Three-dimensional simulation of scour-inducing flow at bridge piers." *Journal of Hydraulic Engineering*, ASCE, Vol. 124, Vol. 5, 530-540.
7. Sicilian, J.M., Hirt, C.W., and Harper, R.P. (1987). FLOW3D: *Computational modeling power for scientists and engineers. FSI-87-00-1*, Flow Science, Los Alamos, NM.
8. Smagorinsky, J. (1963). "General circulation experiments with the primitive equations: I. the basic equations." *Monthly Weather Review*, 91, 2217-2226.

9. Tseng, M., Yen, C.L., and Song, C.C.S. (2000). “Computation of three-dimensional flow around square and circular piers.” *International Journal for Numerical Methods in Fluids*, Vol. 34, 207-227.
10. Versteeg, H.K. and Malalasekera, W. (1995). *An Introduction to Computational Fluid Dynamics*, Longman Group Ltd, Edinburgh, England.
11. Wang, S.Y. and Jia, Y. (2000). “Computational simulations of local scour at bridge crossings-capabilities and limitations.” *International Conference on Hydro-Science Engineering 2000*, CD-ROM.
12. Yakhot, V., Orszag, S.A., Thangam, S., Gatski, T.B., and Speziale, G.G. (1992). “Development of turbulence model for shear flows by a double expansion technique.” *Physics of Fluids*, 4(7), 1510-1520.

Table 1. Grids used in Computation

	Simulation Type	Number of Grids	Grid Dimensions $x \times y \times z$ (m)
LES	w/o scour hole	140,000	0.004×0.002×0.001
	with scour hole	250,000	0.0003×0.002×0.0006
RNG $k-\varepsilon$	w/o scour hole	105,000	0.004×0.005×0.0012
	with scour hole	183,750	0.00098×0.0033×0.0006

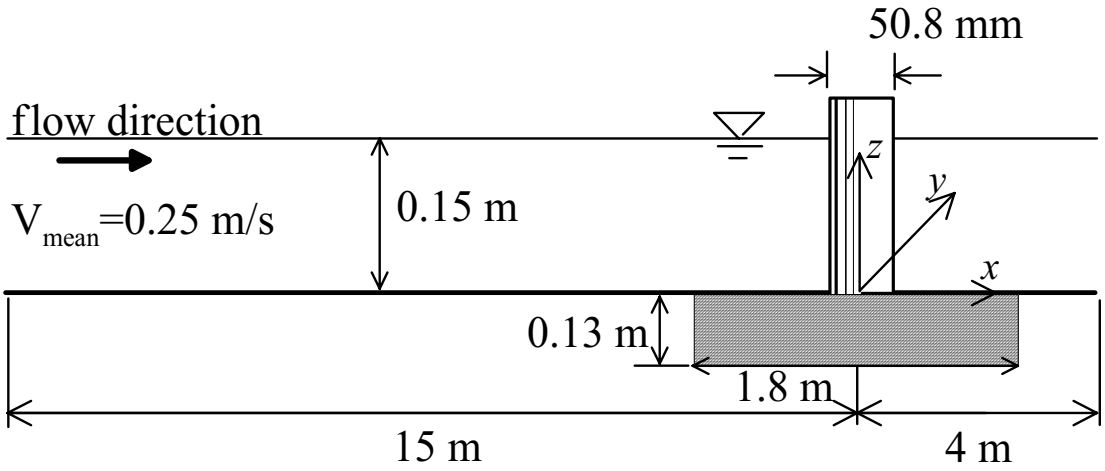

Fig 1. Schematic Figure of Experiments (Melville and Raudkivi, 1977)
(The origin is located at the center of the pier)

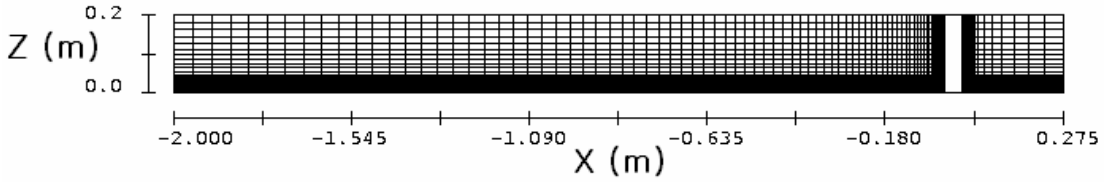

(a) Grid for Simulation without Scour Hole

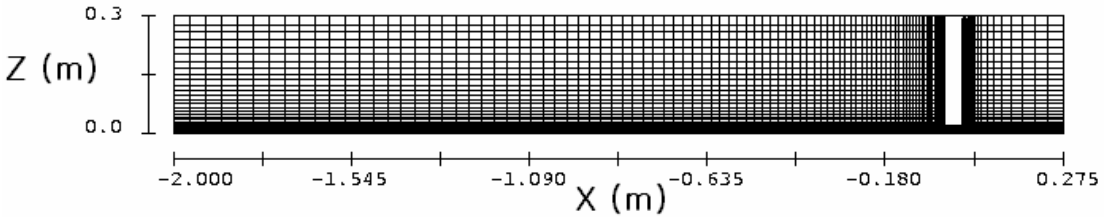

(b) Grid for Simulation with Scour Hole

Fig 2. Grid used in Computation

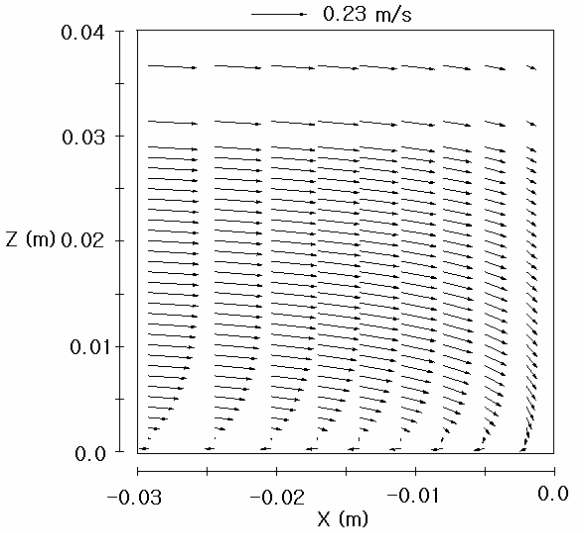

(a) LES

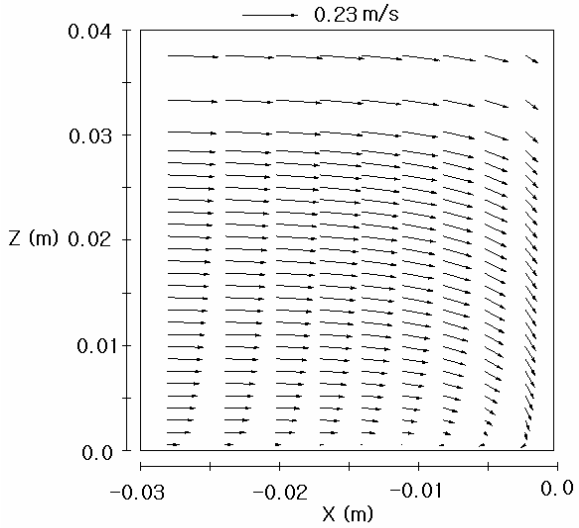

(b) RNG k-ε

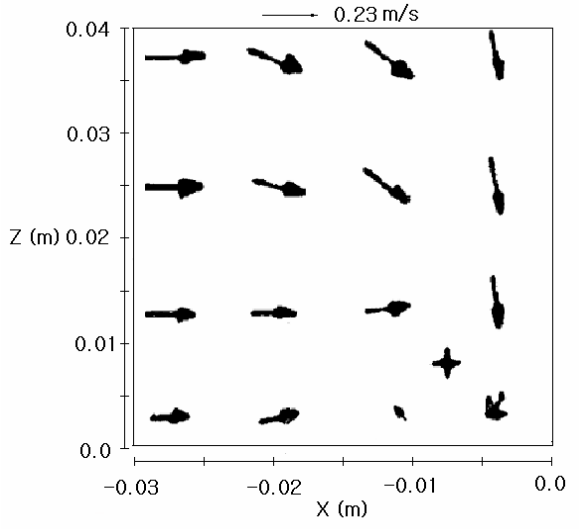

(c) Melville and Raudkivi (1977)

Fig. 3 Velocity Vectors at *x-z* Plane (without Scour Hole)

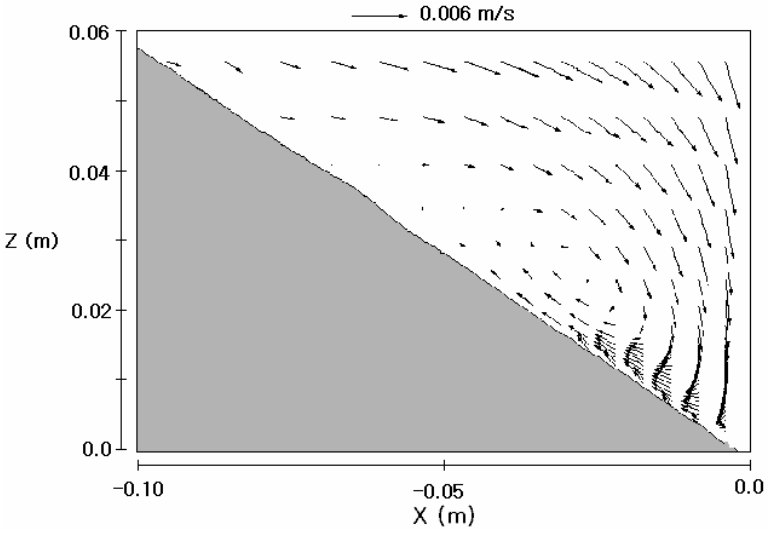

(a) LES

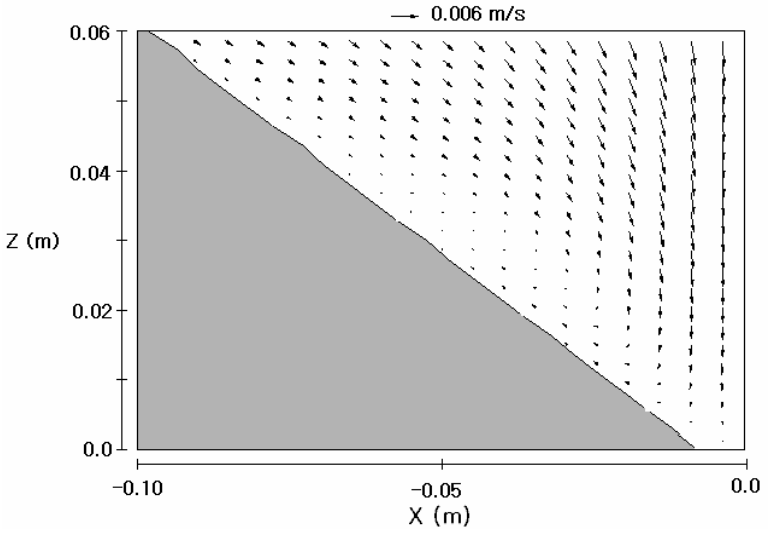

(b) RNG k-ε

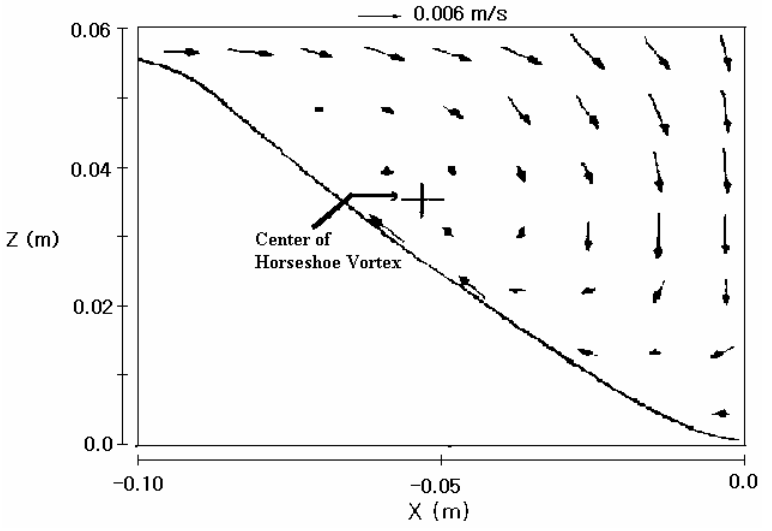

(c) Melville and Raudkivi (1977)

Fig. 4 Velocity Vectors at *y-z* Plane (with Scour Hole)

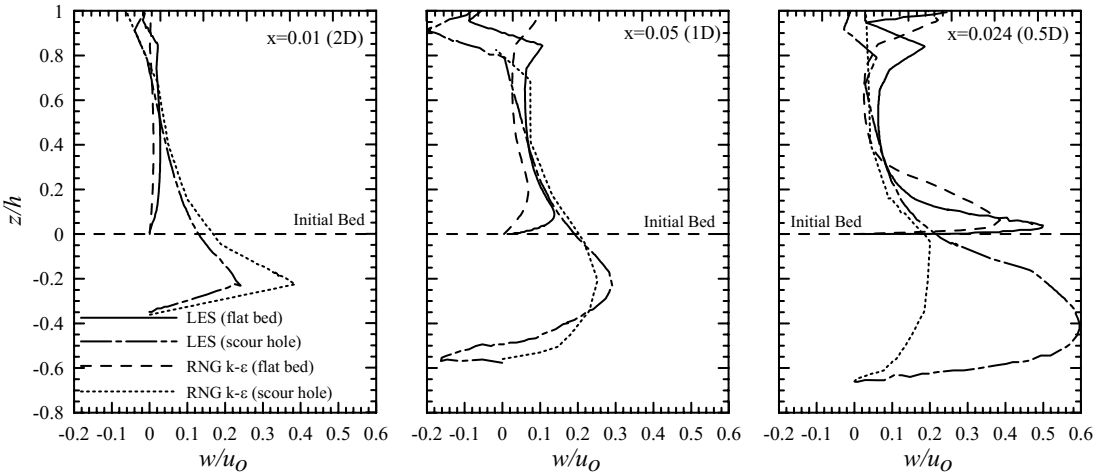

(a) at $x = 2D$ (b) at $x = 1D$ (c) at $x = 0.5D$

Fig 5. Downflow Velocity Profiles at the x-z Plane ($y = 0$)

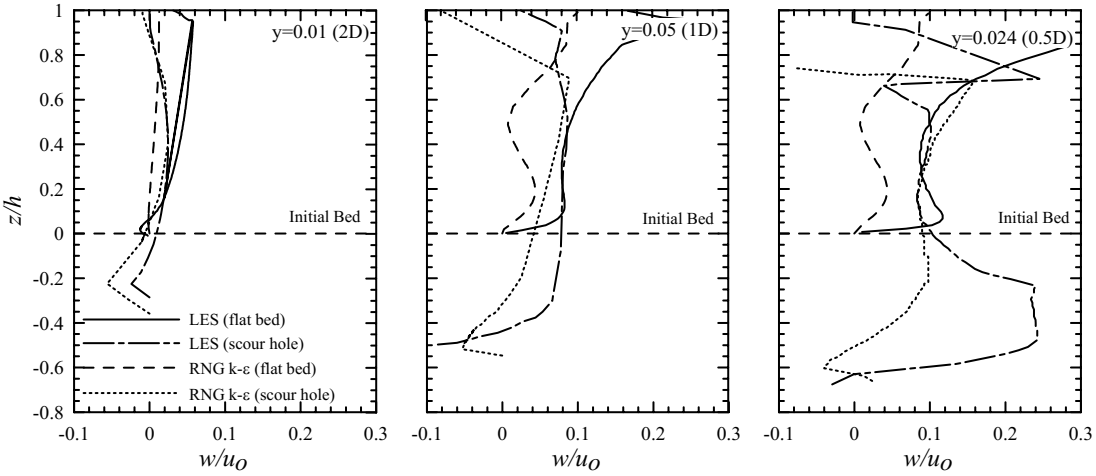

(a) at $y = 2D$ (b) at $y = 1D$ (c) at $y = 0.5D$

Fig 6. Downflow Velocity Profiles at the y-z Plane ($x = 0$)